Freely Diffusing Single Hairpin Ribozymes Provide Insights into the Role of Secondary Structure and Partially Folded States in RNA Folding

Goran Pljevaljčić, David P. Millar, and Ashok A. Deniz
The Scripps Research Institute, Department of Molecular Biology, La Jolla, California

ABSTRACT Single-molecule fluorescence resonance energy transfer studies of freely diffusing hairpin ribozymes with different combinations of helical junction and loop elements reveal striking differences in their folding behavior. We examined a series of six different ribozymes consisting of two-, three- and four-way junction variants, as well as corresponding constructs with one of the two loops removed. Our results highlight the varying contributions of preformed secondary structure elements to tertiary folding of the hairpin ribozyme. Of the three helical junction variants studied, the four-way junction strongly favored folding to a docked conformation of the two loops, required for catalytic activity. Moreover, the four-way junction was uniquely able to fold to a similar compact structure even in the absence of specific loop-loop docking interactions. A key feature of the data is the observation of broadening/tailing in the fluorescence resonance energy transfer histogram peak for a single-loop mutant of the four-way junction at higher Mg^{2+} concentrations, not observed for any of the other single-loop variants. This feature is consistent with interconversion between compact and extended structures, which we estimate takes place on the 100-μs timescale using a simple model for the peak shape. This unique ability of the four-way junction ribozyme to populate an undocked conformation with native-like structure (a quasi-docked state) likely contributes to its greater tertiary structure stability, with the quasi-docked state acting as an intermediate and facilitating the subsequent formation of the specific hydrogen bonding network during docking of the two loops. The inability of two- and three-way junction ribozymes to fully populate a docked conformation reveals the importance of correct helical junction geometry as well as loop elements for effective ribozyme folding.

INTRODUCTION

Ribonucleic acid (RNA) folding represents a critical step toward the generation of functional three-dimensional structures of RNA molecules. Although some RNA molecules have been observed to fold quite rapidly (100-ms timescale) (Fang et al., 1999), much slower folding is generally observed, especially for large RNAs with complex tertiary structures (Treiber and Williamson, 1999, 2001). Current models of RNA folding propose distinguishable early and late events during RNA structure formation (Sosnick and Pan, 2003). Rapid early events may lead either to a nonspecific RNA compaction, comparable to molten globule formation during protein folding (Buchmueller et al., 2000; Russell et al., 2000, 2002b), or to compact structures with partially formed subdomains of tertiary structure (Fang et al., 1999, 2002). Subsequently, the native tertiary structure is formed through a slow (rate-limiting) conformational search and/or consolidation of specific metal-ion binding sites. These fundamental aspects of RNA folding are frequently obscured by the strong tendency of RNA to form alternate secondary or tertiary structures, which act as kinetic traps and retard the overall rate of folding.

The folding of RNA is generally coupled to its biological function, and this is illustrated well by the hairpin ribozyme, a small catalytic RNA with both endonuclease and ligase activities. The natural ribozyme is comprised of a four-way helical junction (4WJ) and two loops (A and B), carried on two adjacent helical arms (Fig. 1). During cleavage or ligation, the two loops are required to interact, which comes about through a magnesium-dependent folding transition that places the loops in close physical proximity (Murchie et al., 1998; N. G. Walter et al., 1998). The resulting network of tertiary loop-loop contacts are revealed in a crystal structure of the hairpin ribozyme in its docked conformation (Rupert and Ferre-D'Amare, 2001). Docking of the two loops is also observed in simpler ribozyme constructs comprised of two- or three-way helical junctions (2WJ and 3WJ, respectively), although much higher Mg^{2+} concentrations are required (N. G. Walter et al., 1999). Hence, the helical junction geometry strongly affects the tertiary folding of the hairpin ribozyme.

Fluorescence resonance energy transfer (FRET) is a very informative technique for studying the tertiary folding of the hairpin ribozyme. Steady-state FRET methods were first used to monitor the docking of loops A and B during magnesium-induced folding (N. G. Walter et al., 1998) and to elucidate the global geometry of the hairpin ribozyme in docked and extended states (Murchie et al., 1998), as well as the four-way helical junction from which it is derived (F. Walter et al., 1998). Time-resolved FRET (trFRET) measurements were subsequently used to resolve and quantify the equilibrium distribution of extended and docked ribozyme conformers (N. G. Walter et al., 1999). These studies have provided thermodynamic information on the global folding of the hairpin ribozyme (Klostermeier and Millar, 2000) and also quantified the energetic contributions

Submitted October 15, 2003, and accepted for publication March 5, 2004.

Address reprint requests to Ashok A. Deniz, E-mail: deniz@scripps.edu; or David P. Millar, E-mail: millar@scripps.edu.

0006-3495/04/07/457/11 $2.00

doi: 10.1529/biophysj.103.036087

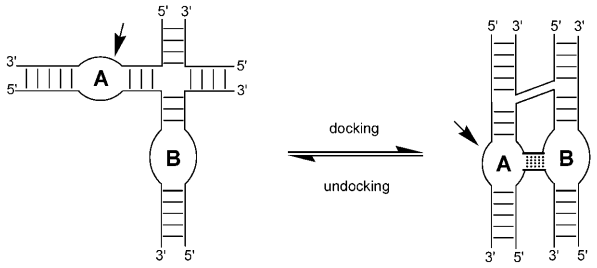

FIGURE 1 Schematic representation of the hairpin ribozyme docking process occurring upon addition of Mg^{2+} ions, showing loops *A* and *B* that form specific tertiary hydrogen bonding interactions. The arrow marks the potential cleavage site within loop *A*, which is blocked in the present studies by a 2′-deoxy modification of A_{-1}.

of individual tertiary interactions (Klostermeier and Millar, 2001a, 2002).

Single-molecule methods represent an excellent tool to decipher the complexity of RNA folding processes, which generally proceed via intermediates and multiple pathways. These intrinsic features of RNA folding reactions can be obscured due to the averaging inherent in conventional ensemble experiments. Single-pair FRET (spFRET) measurements can provide new insights into the details of RNA folding processes, by virtue of their enhanced abilities to report distributions and dynamics of molecular conformations (Ha et al., 1999; Zhuang et al., 2000; Russell et al., 2002a; Zhuang et al., 2002). To date, such studies have been carried out using charge-coupled device camera or avalanche-photodiode detection of surface-immobilized RNA molecules, including a minimal (2WJ) form of the hairpin ribozyme (Zhuang et al., 2002) and the natural ribozyme containing a 4WJ (Tan et al., 2003).

A complementary approach is to characterize the conformational distributions of freely diffusing RNA molecules using a single-molecule method referred to as diffusion spFRET (Deniz et al., 2001). In this method, the fluorescence of donor and acceptor are simultaneously recorded using avalanche-photodiodes as individual molecules traverse the excitation volume in a confocal microscope, and the FRET efficiencies from many such single-molecule observations are plotted in the form of a histogram. The resulting histogram can directly reveal conformational subpopulations that are averaged in conventional ensemble FRET measurements. In addition, kinetic information on subpopulations interconverting on the microsecond to millisecond timescales can be obtained from a detailed analysis of the FRET histogram peak shapes. Kinetic information on this timescale has not been available from charge-coupled device camera imaging of immobilized molecules, where the time resolution has typically been limited to tens of milliseconds.

In the first application of diffusion spFRET to study RNA folding, we have investigated the magnesium-induced tertiary folding of the hairpin ribozyme. Using the hairpin ribozyme as a model system, we specifically address a key question in RNA folding—how do preformed secondary structure elements dictate the course of subsequent tertiary folding events? Currently, little is known about how secondary structural elements affect the ribozyme conformational distributions important in the course of folding. The hairpin ribozyme is a good model to explore this question because of the relatively simple secondary structure and the strong dependence of tertiary folding on the helical junction geometry. Here we present a systematic study of the folding behavior of hairpin ribozymes containing different combinations of loop and helical junction elements. Our results illustrate how these secondary structure elements combine to direct the tertiary folding pathway of the ribozyme.

MATERIALS AND METHODS

RNA constructs

2′-*O*-bis(2-acetoxyethoxy)methyl orthoester (2′-ACE) protected RNA strands were purchased from Dharmacon (Boulder, CO). The sequences are 5′-Cy3 AAA UAG AGA AGC GAA CCA GAG AAA CAC ACG CC-3′ (2WJ/3WJ/4WJ), 5′-Cy5 GGC GUG GUA CAU UAC CUG GUA CCC CCU CGC ***d***AGU CCU AUU U-3′ (2WJ), 5′-Cy5 GGC GUG GUA CAU UAC CUG GUA CGA GUU GAC-3′ (3WJ/4WJ/4WJ single-loop (SL)), 5′-GUC AAC UCG UUC GC***d***A GUC CUA UUU-3′ (3WJ), 5′-GCA AGC CAC CUC GC***d***A GUC CUA UUU-3′ (4WJ), 5′-GUC AAC UCG UGG UGG CUU GC-3′ (4WJ/4WJ SL), 5′-Cy5 GGC GUG GUA CAU UAC CUG GUA CCC CCU CGC GAG CCU AUU U-3′ (2WJ SL), 5′-GCA AGC CAC CUC GCG AGC CUA UUU-3′ (4WJ SL) and 5′-Cy3 AAA UAG GCU CGC GAA CCA GAG AAA CAC ACG CC-3′ (2WJ & 4WJ SL). A deoxy adenosine residue was incorporated at the potential cleavage site in the strands shown above to prevent actual strand cleavage during the fluorescence measurements. For the activity assays (see below), the substrate strand sequences used are 5′-GGC GUG GUA CAU UAC CUG GUA CCC CCU CGC AGU CCU A-3′ (S2WJ), 5′-GUC AAC UCG UUC GCA GUC CUA-3′ (S3WJ) and 5′-GCA AGC CAC CUC GCA GUC CUA-3′ (S4WJ). The RNA strands were deprotected, purified by denaturing urea gel electrophoresis, desalted and subsequently purified by reversed-phase high-performance liquid chromatography utilizing an eluent system of acetonitrile and aqueous triethylammonium acetate (100 mM, pH 7). Ribozyme constructs were prepared in 50 mM Tris/HCl (pH 7.5), 100 mM NaCl (referred to as annealing buffer) at a concentration of 1 μM donor strand, 5 μM acceptor strand, and 10 μM of additional strands (if applicable) and were annealed by heating to 70°C for 2 min and cooling to ambient temperature. For diffusion spFRET measurements, the resulting ribozyme complexes were diluted with annealing buffer (missing NaCl and supplemented with 0.5 mM oxygen scavenger propyl galate (Grunwell et al., 2001)) to a final concentration of 100 pM RNA (in terms of donor strand).

Hairpin ribozyme activity assay

The substrate strands S2WJ, S3WJ, and S4WJ were labeled radioactively with ^{32}P at the 5′ terminii. Each substrate strand (20 pmole) was incubated with γ^{32}ATP (125 pmoles) and T4 polynucleotide kinase (10 U) in 70 mM Tris-HCl (pH 7.6), 10 mM $MgCl_2$, and 5 mM dithiothreitol for 30 min at 37°C. Subsequently, the strands were purified using sephadex G-25 quick spin columns (Roche, Basel, Switzerland). Ribozyme constructs missing the substrate strand were prepared in annealing buffer (missing NaCl and supplemented with 12 mM $MgCl_2$) at a concentration of 2 μM of each strand and annealed by heating to 70°C for 2 min and cooling to ambient temperature. The cleavage reaction was initiated by addition of substrate strands (500 pM) to the respective preformed ribozyme complex (100 nM) at

room temperature and reaction progress was monitored by gel analysis of aliquots quenched with formamide at different time points. Denaturing urea gel electrophoresis followed by quantification of RNA bands using phosphorimager analysis and determination of the ratio of cleaved to uncleaved substrate strand as a function of time provided ribozyme activity information.

spFRET measurements and data analysis

Single-molecule measurements and data analysis were performed as described previously (Deniz et al., 1999, 2001). Briefly, fluorescence measurements were carried out using a home-built laser confocal microscope system, based around an Axiovert 200 microscope (Zeiss, Thornwood, NY). Excitation was achieved by focusing the 514-nm line of a 543-AP-A01 tunable argon-ion laser (Melles Griot, Carlsbad, CA) inside the sample solution, 10 μm from the glass coverslip surface, using a Plan Apo 100×, 1.4 NA oil immersion objective (Zeiss). The fluorescence emission was collected using the same objective, separated from the excitation light using a dichroic filter (540 DRLP, Omega Optical, Brattleboro, VT), spatially filtered using a 100-μm pinhole, and separated into donor and acceptor components using a second dichroic filter (630 DRLP, Omega Optical). The donor and acceptor signals were further filtered using an HQ585/60m band-pass filter (donor, Chroma Technology Corp., Rockingham, VT) and a 640AELP long-pass filter (acceptor, Omega Optical), then detected using SPCM-AQR-14 avalanche photodiodes (Perkin-Elmer Optoelectronics, Fremont, CA), and the signals were recorded using a photon counting card (PCI 6602, National Instruments, Austin, TX) and computer. The FRET efficiency histograms described in this article were generated by using a two-channel data collection mode to simultaneously record donor and acceptor signals as a function of time, with a time resolution of 0.5 ms. The donor-acceptor solutions used were 100 pM in donor concentration, ensuring that virtually all of the detected signals were due to single molecules. The signals were corrected for average background due to buffer, the effects of Cy3 leakage into the Cy5 channel, and direct excitation of Cy5 at 514 nm. A threshold of 40 counts (sum of signals from the two channels) was then used to separate fluorescence signals from background, and FRET efficiencies were calculated for each accepted event using the equation $E = (1 + \gamma I_d/I_a)^{-1}$, and plotted in the form of a histogram. For the purpose of this article, we have used a value of 1 for the correction factor γ, which is a ratio of the products of fluorescence quantum yield and the instrument detection efficiency in the two channels. Since we use relative peak positions and distance (inter-arm proximity) changes in our discussion here (and not absolute distances), variations of γ from 1 do not affect the discussion or conclusions of this study. We note that variations of γ as a function of solvent could potentially produce shifts in peak position in the histograms. This issue and appropriate control experiments are discussed further in the Results section. FRET histograms were fit with multiple Gaussian functions using Origin (OriginLab Corp., Northampton, MA), and the peak position (E^{peak}) and relative areas of individual peaks were calculated from the fitting parameters. For most of the peaks in the histograms, the peak position (E^{peak}) from these fits is a good approximation for the mean E for the peak, due to their fairly symmetric shapes. In the case of the SL 4WJ, for the broad/asymmetric peaks at some of the high Mg^{2+} concentrations, these fitted E^{peak} values are representative of the peak positions, but are higher than the average FRET efficiencies by ~0.1 units.

For the WT ribozymes, docked fractions (F) were calculated as a ratio of docked/undocked areas (A) as, $F = A^{docked}/(A^{docked} + A^{undocked})$(Deniz et al., 2001). These fractions were plotted versus Mg^{2+}concentration and fitted to the cooperative binding equation $F = F^{max}([Mg]^n/([Mg]^n + (K_D^{Mg})^n))$, to yield an apparent dissociation constant $K_D^{Mg}$for Mg^{2+}, and an apparent cooperativity coefficient, n.

The average burst duration for the SL 4WJ at 10mM Mg^{2+} was estimated from two-channel data acquired with time bins of 50 μs, by averaging the burst durations within each 500-μs rebinned point lying above a threshold of 40. In this procedure, the 50 μs data was first rebinned in 500-μs time bins, and rebinned data points lying above a threshold of 40 counts were identified (i.e., under conditions used for generating the FRET histograms in this article). For each of these identified points, the constituent 50-μs binned data was then used to calculate the ''burst duration'' during this time bin, by determining the total time spent above a threshold of 4 counts.

FRET histogram simulations

FRET histogram simulation routines were written in Matlab (The MathWorks, Natick, MA). For histogram simulations of the SL 4WJ at 10 mM Mg^{2+}, the state of the ribozyme system was allowed to stochastically switch between the extended undocked and quasi-docked states according to the assumed forward and reverse rate constants (see Fig. 10). The rate constants were expressed in units of an experimental reference time, the average burst duration, as discussed later. The E values of the extended undocked and quasi-docked conformations were set to 0.25 and 0.95, respectively, based on the observed endpoints in the E shifts in Fig. 8 *C*. The ribozyme system is sampled at 40 times per measurement interval to simulate the effects of the threshold of 40 photons we used for the FRET analysis. At each sampling time, the state of the system is queried, and the recorded photon is assigned to either donor or acceptor channel, with a probability based on the FRET efficiency of the detected system state. Such a procedure takes into account the shot noise-induced broadening of the peak (Deniz et al., 1999; Dahan et al., 1999), as well as additional broadening due to interconversion between different conformations. Other potential experimental sources of broadening, such as dark states or photobleaching, are not considered in these simple simulations. The simulation is run for 20,000 such 40-photon events, and the FRET efficiency histogram is then plotted as described previously.

RESULTS

spFRET histograms reveal subpopulations of docked and extended ribozyme conformers

Fluorescence resonance energy transfer (FRET) is the nonradiative transfer of excitation energy between donor and acceptor dyes with overlapping emission and absorption spectra. The efficiency E of this process exhibits a strong distance dependence, given by $E = 1/(1 + (R/R_0)^6)$, where R is the donor-acceptor distance and R_0 is the Förster radius at which the efficiency is 50%. This distance dependence has been experimentally verified under ensemble conditions (Stryer and Haugland, 1967). More recently, single-molecule FRET detection (Ha et al., 1996) and distance dependence measurements (Deniz et al., 1999) have also been demonstrated. The distance dependence of the FRET efficiency provides a very sensitive fluorescence-based measure of distances in the 20–80 Å range. This feature of FRET has been used extensively to study the structure and dynamics of biological molecules and assemblies, in ensemble as well as more recent single-molecule measurements (Selvin 2000; Klostermeier and Millar, 2001b; Weiss, 2000; Ha, 2001). In the diffusion spFRET measurements described in this article, by labeling the ends of the loop-bearing arms with donor and acceptor dyes, we use the FRET efficiency E as an indicator of the distance between arms A and B of the ribozyme during the docking process. The loops on these arms interact closely

upon docking, making E a good measure of the docking coordinate.

Fig. 3 *A* shows fluorescence signals from freely diffusing ribozyme molecules labeled with Cy3 (donor) and Cy5 (acceptor) at 0.1 mM Mg^{2+}. The ribozyme construct contains the naturally occurring 4WJ (Fig. 2 *C*). Intense bursts of fluorescence are observed occasionally from donor and/or acceptor above the low background (trace shown in Fig. 3 *A* for comparison), and these bursts are analyzed to generate a FRET histogram (Fig. 3 *B*) as described in the Materials and Methods section. A peak close to zero FRET efficiency is always observed, and occurs in part due to photobleaching of the acceptor, as well as other processes that give rise to donor-only molecules (Deniz et al., 1999). Because this peak does not provide relevant FRET (distance) information, only the region above $E = 0.1$ is displayed in subsequent histograms. The histogram shows two well-resolved (non-zero) peaks, centered at $E \sim 0.25$ and $E \sim 0.85$, corresponding to donor-acceptor distances of ~64 Å and 40 Å, respectively. The observation of well-resolved subpopulations in the FRET efficiency histogram indicates that the ribozyme can adopt two distinct conformations in solution. Because the donor and acceptor are attached to the ends of the loop-bearing arms, a short donor-acceptor distance is expected if the two loops are in a docked conformation. Hence, we assign the high E peak to such a docked species. Additionally, since the low E peak indicates a species with a longer inter-arm distance, we assign this peak to an extended (undocked) conformation. To confirm these assignments, we examined a destabilized 4WJ ribozyme variant, in which G_{11} is replaced by inosine (I). This mutation eliminates a tertiary hydrogen bonding interaction between G_{11} (loop A) and A_{23} (loop B) and is expected to destabilize the docked conformer (Rupert and Ferre-D'Amare, 2001; Klostermeier and Millar, 2002). The FRET efficiency histogram of the G_{11}I variant also exhibits two distinct subpopulations, with mean E values that are similar to the wild-type, but the amplitude of the high FRET peak is substantially reduced relative to the low FRET peak (Fig. 4). Hence, the high- and low-E peaks can be assigned to docked and extended ribozyme conformers, respectively.

Since the docked and undocked peaks are well resolved, any interconversion between the two conformers must occur more slowly than the ~280-μs average burst duration of the single-molecule measurements (see below). If instead, subpopulations interconvert rapidly on the burst-duration timescale, a single averaged peak will be observed, with increased broadening as the interconversion rate approaches this timescale. Hence, peak properties can be used to directly monitor the characteristics of individual molecular subpopulations under different solution conditions.

Influence of helical junction geometry on docking efficiency

We obtained FRET efficiency histograms for three ribozyme constructs with different helical junction geometries (natural 4WJ as well as corresponding 2WJ and 3WJ constructs; Fig. 2) over a wide range of Mg^{2+} concentrations. Fig. 5 shows selected histograms from these measurements from 0.01 to 10 mM Mg^{2+}. At low Mg^{2+}, all three ribozymes show a single peak at low E, reflecting an extended, undocked state. A high FRET peak, characteristic of a compact, docked state, grows in at higher Mg^{2+} concentration. We note that the term ''compact'' is used in this article to denote the proximity of arms A and B, as described by the FRET efficiency for the current labeling scheme. By fitting the peaks in the histograms with Gaussian functions, we characterize their properties, such as peak position, relative areas of the peaks, and peak shapes as described in the Materials and Methods section. Docked fractions calculated from relative areas of the peaks are plotted in Fig. 6 as a function of Mg^{2+}. These data were fitted with a cooperative binding model, and the resulting fits are shown as solid lines in Fig. 6. The apparent dissociation constants for Mg^{2+} (K_D^{Mg}) recovered from the fits are 2.11 ± 0.33 mM (2WJ), 1.22 ± 0.26 mM (3WJ), and 0.22 ± 0.03 mM (4WJ). The cooperativity coefficients (n) are all close to unity: 1.29 ± 0.16 (2WJ), 1.41 ± 0.32 (3WJ), and 1.02 ± 0.14 (4WJ), suggesting that the docking of these ribozyme constructs is coupled to the binding of a single Mg^{2+} ion. The 4WJ ribozyme docks with the highest efficiency, i.e., at the lowest

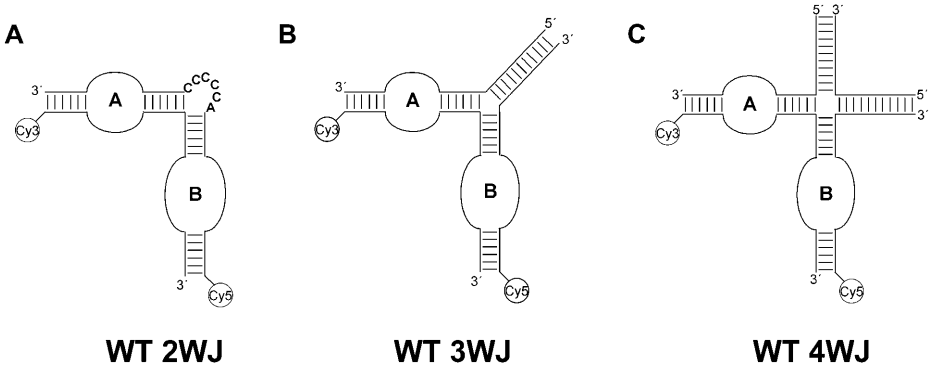

FIGURE 2 Wild-type hairpin ribozyme constructs used in ratiometric spFRET studies. (*A*) Minimal two-way helical junction (*WT 2WJ*); (*B*) three-way helical junction (*WT 3WJ*); and (*C*) natural four-way helical junction (*WT 4WJ*). Donor fluorophore Cy3 and acceptor fluorophore Cy5 are attached to the loop-bearing arms in each case via the 5′ ends of the appropriate RNA strands (see Materials and Methods for details).

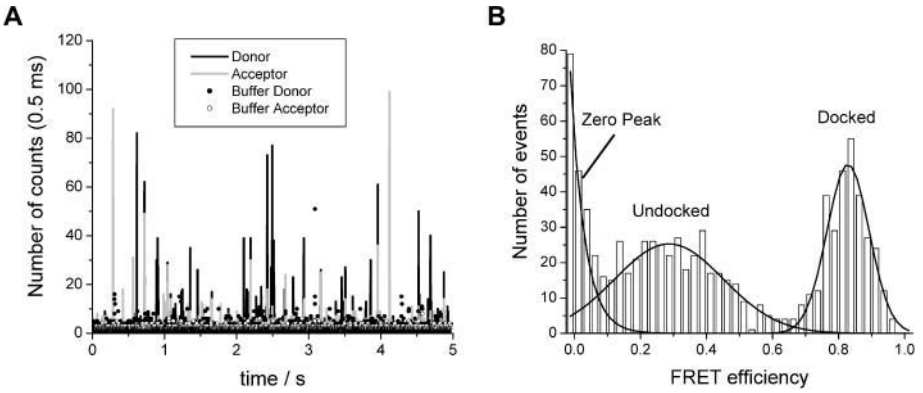

FIGURE 3 Ratiometric spFRET data for the WT 4WJ ribozyme. (*A*) Example of donor (*black*) and acceptor (*gray*) emission bursts observed in spFRET experiments. A time trace is presented for the WT 4WJ ribozyme at a concentration of 100 pM in 50 mM Tris/HCl buffer with 0.1 mM Mg^{2+} at room temperature, and the data integration time per point was 0.5 ms. Fluorescent donor and acceptor bursts are observed above background. A buffer (background) time trace is also shown for comparison. Only bursts above a threshold of 40 counts (sum of donor and acceptor signals) were used to construct FRET efficiency histograms. (*B*) FRET efficiency histogram derived from calculation of FRET efficiencies from each accepted donor/acceptor event above a threshold of 40 counts, showing the docked and undocked subpopulations (see text), as well as the zero-*E* peak. The solid lines show fits using Gaussian functions.

Mg^{2+} concentration. Additionally, only this ribozyme is almost completely docked at physiological concentrations of Mg^{2+} (~2 mM).

To confirm that our labeled ribozyme constructs are active in cleavage, we performed activity assays using a cleavable all-RNA substrate strand, as described in the Materials and Methods section. We found that all three constructs were active in cleavage, and that the cleavage half-lives were 21.2, 29.2, and 26.1 min for the wild-type (WT) 2WJ, 3WJ, and 4WJ ribozymes, respectively.

Folding of single-loop ribozyme constructs

The results described in the preceding section suggest that Mg^{2+}-induced conformational changes within the helical junction region may control the approach of loops A and B during ribozyme folding. To isolate the contribution of the helical junctions to tertiary folding, we also studied the corresponding ribozyme constructs without the loop on arm A (SL 2WJ, 3WJ, and 4WJ, Fig. 7, *upper panel*), thereby preventing specific loop-loop interactions. The loss of these specific tertiary docking interactions makes these SL constructs mimics for the undocked state of the corresponding WT ribozymes. All SL constructs show just a single peak in the FRET efficiency histograms, with no distinct docked peak, as expected (Fig. 7, *lower panel*). Fig. 8 shows a comparison of the peak positions for the SL and WT versions of the ribozymes. The peak positions for the SL 2WJ and 3WJ constructs closely follow the trends observed for the undocked peak with the corresponding WT constructs, confirming that removal of the loop on arm A provides appropriate models for the undocked states of the WT ribozymes.

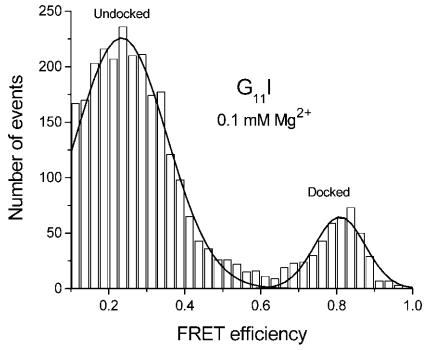

FIGURE 4 FRET efficiency histogram for a $G_{11}I$ mutant of the 4WJ ribozyme at 0.1 mM Mg^{2+}, using the same conditions as for data presented in Fig. 3. Solid lines show fits using Gaussian functions. The relative area of the high efficiency (docked) peak is markedly reduced relative to the wild-type 4WJ ribozyme (Fig. 3), reflecting a destabilized tertiary structure for the mutant.

The peak position for the SL 3WJ remains in the low-FRET region of the histograms, independent of the Mg^{2+} concentration, indicating that this ribozyme construct is incapable of folding to a compact structure (Fig. 8 *B*). The SL 2WJ shows a small but marked peak shift to higher *E* as Mg^{2+} concentration is increased (Fig. 8 *A*), indicating shifts in a broad conformational ensemble, with arms A and B coming closer on average. In contrast, the SL 4WJ shows a dramatic shift from very low *E* (0.25) at low Mg^{2+}, to above 0.9 at high Mg^{2+} (Fig. 8 *C*). Hence, the 4WJ ribozyme is unique in its ability to fold into a structure with arms A and B in close proximity, similar to the native ribozyme, even in the absence of specific loop-loop docking interactions. We refer to this species as a quasi-docked state to denote the native-like arrangement of arms A and B, although there are no actual docking interactions between these arms because loop A is absent.

We note here that although we have interpreted peak shifts and broadening in terms of distance changes and ribozyme subpopulations, respectively, peak shifts could also potentially be caused by solvent effects on dye photophysics, and corresponding changes in the correction factor γ (see Materials and Methods), as well as peak broadening by effects of κ^2, the orientation factor (Deniz et al., 2000). However, because we have compared results

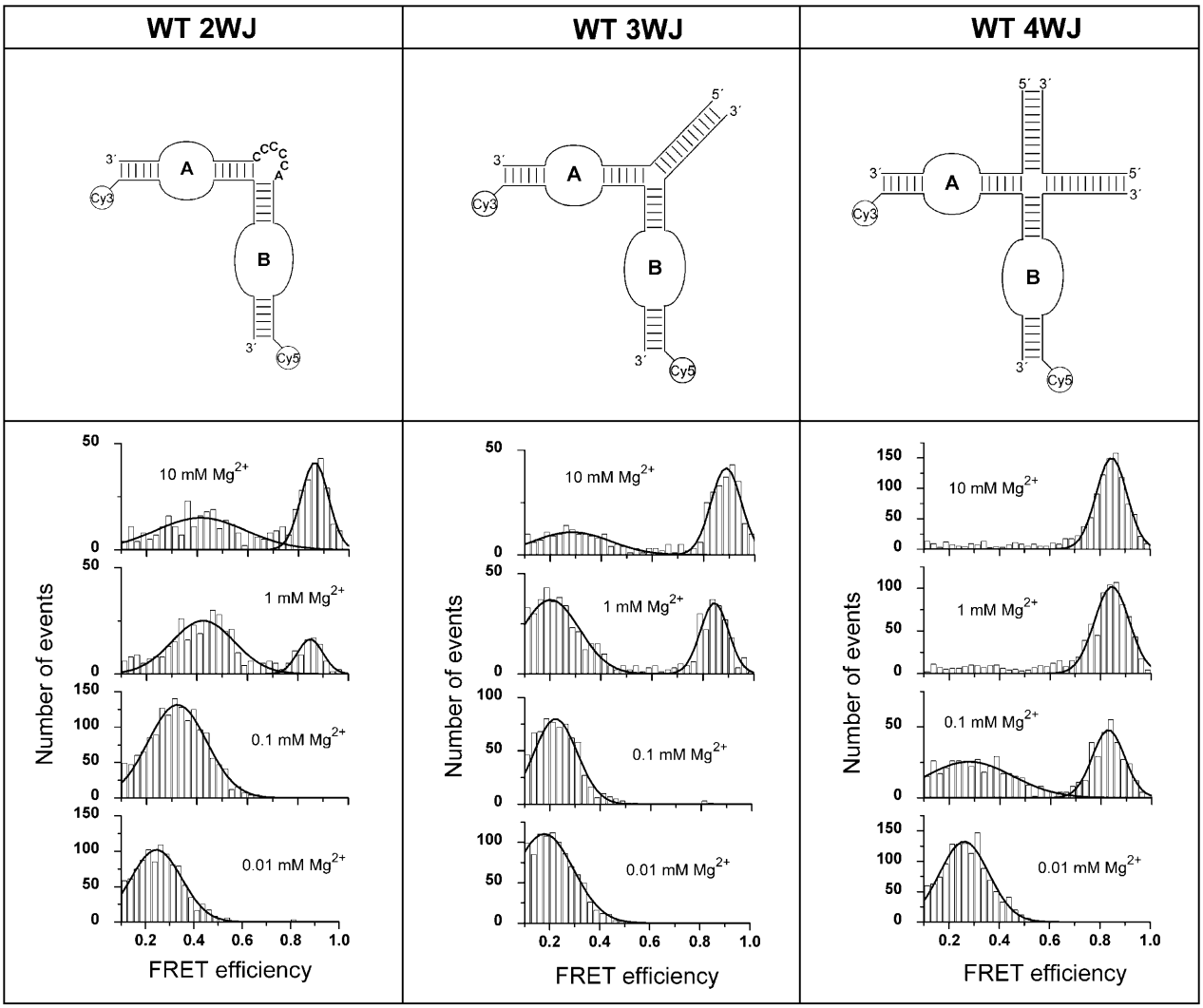

FIGURE 5 Schematic representation of WT ribozyme constructs used for spFRET studies (*upper panel*). FRET efficiency histograms (*bars*) for wild-type 2WJ, 3WJ, and 4WJ hairpin ribozymes, showing undocked and docked ribozyme subpopulations at Mg^{2+} concentrations of 0.01, 0.1, 1, and 10 mM (*lower panel*). Data were acquired using a ribozyme concentration of 100 pM in 50 mM Tris/HCl buffer with Mg^{2+} at room temperature, and the data integration time per point was 0.5 ms. The smooth lines show fits using Gaussian functions.

across a series of molecules where the RNA sequence (and secondary structure) in the vicinity of the dyes has been held constant, the differences between the characteristics we observe are related primarily to tertiary structural differences between the constructs. To further evaluate the contribution of solvent-induced shifts, we examined a model duplex DNA molecule whose structure is not expected to change significantly with Mg^{2+} concentration changes in the 0.01–10 mM Mg^{2+} range. This duplex has a 14-bp separation between donor and acceptor, and spFRET experiments show only a small change in E upon going from 0.01 mM to 1 M Mg^{2+}. These data are overlaid on the shift plots in Fig. 8 *B* for comparison. This result confirms that the sizable increases in E with Mg^{2+} that we observe for the 2WJ (WT and SL) and SL 4WJ ribozymes are due to decreases in the interarm distances.

Evidence for rapid interconversion of extended and quasi-docked ribozyme conformations

A notable feature of the SL 4WJ in the presence of high Mg^{2+} concentrations is the markedly asymmetric peak shape in the FRET efficiency histogram, with pronounced tailing on the low-E side of the peak (Fig. 9 *A*). The relatively narrow and symmetric peak observed for the WT 4WJ under the same conditions is overlaid for comparison. This broadening/tailing is evidence for occupation of two (or more) structures that are interconverting on a timescale similar to or slower than the average burst duration. Taken together, the smooth E shifts with changing Mg^{2+} concentration combined with the observed broadening/tailing at high Mg^{2+} concentration are consistent with the presence of a dynamic equilibrium between the quasi-docked

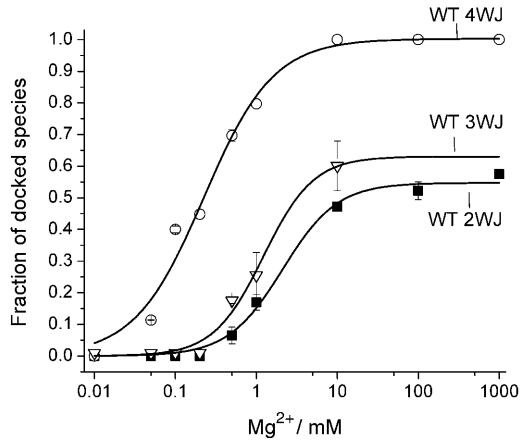

	F^{max}	K_D^{Mg} / mM	n
WT 2WJ	0.55 ± 0.02	2.11 ± 0.33	1.29 ± 0.16
WT 3WJ	0.63 ± 0.04	1.22 ± 0.26	1.41 ± 0.32
WT 4WJ	1.00 ± 0.03	0.22 ± 0.03	1.02 ± 0.14

FIGURE 6 Effect of helical junction geometry on magnesium-induced docking of the hairpin ribozyme. Fractions of docked 2WJ (■), 3WJ (▽), and 4WJ (○) hairpin ribozymes are plotted as a function of Mg^{2+} concentration. The best-fit values of the parameters F^{max}, K_D^{Mg}, and n, obtained from fitting to a cooperative binding equation, are indicated below the graph. Errors represent single standard deviations.

state and an extended undocked state, with a relatively small energy barrier for interconversion (Fig. 10). To better understand the basis for the observed broadening and tailing, we carried out numerical simulations using a simple model of the single-molecule FRET data. The simulations incorporate peak broadening due to interconversion of the proposed extended undocked and quasi-docked conformations (Fig. 10), as well as an upper limit on the intrinsic statistical broadening of the FRET histograms due to shot noise (Deniz et al., 1999; Dahan et al., 1999). The E values of these two conformations were set to 0.25 and 0.95, respectively, based on the observed endpoints in the E-shifts in Fig. 8 *C*. In the simulations, the interconversion rate constants are defined in comparison with an experimental reference time. We define this reference time as the average burst duration within the 0.5-ms time bins that we have used for the FRET histogram data. Using 50-μs time bins and a threshold of 4 counts, we calculate the average burst duration to be ~280 μs.

Using these simulations, we find that the shapes of the histograms are significantly altered by modest changes (twofold) in the interconversion rate constants or their ratio (equilibrium constant). In Fig. 9 *B*, we plot a simulated histogram (*bold line*) using an equilibrium constant of 3 (in favor of the quasi-docked conformation), and forward and reverse rate constants of 20×10^3 and 6.8×10^3 s^{-1}, respectively. The overlay with the experimental data (*bars*) shows that the simulations describe the data fairly well, given the simplicity of the model. For comparison, we also overlay histograms for twofold slower and faster rate constants (*dashed lines*), with the equilibrium constant maintained at 3. Clearly, these simulations do not describe the data as well. We have also tested equilibrium constants of 1.5 and 6, and several corresponding pairs of rate constants (data not shown), and find these to be poorer descriptions of the experimental data as well. Thus, within the framework of these simulations and the two-state model, we can estimate the forward rate constant (k_1) for the extended-undocked to quasi-docked reaction to be in the 10×10^3–41×10^3 s^{-1} range and the reverse rate constant (k_{-1}) in the 3.4×10^3–14×10^3 s^{-1} range.

DISCUSSION

Comparison of spFRET histograms and ensemble trFRET measurements

Our spFRET results for the wild-type ribozymes show the presence of extended (undocked) and docked conformations, with relative populations that are strongly dependent on the Mg^{2+} concentration. Extended and docked conformations of the hairpin ribozyme were also resolved and quantified in previous ensemble trFRET experiments (N. G. Walter et al., 1999). The trFRET method permits the spectroscopic resolution of an equilibrium mixture of alternate RNA conformers from an analysis of the effect of energy transfer to the acceptor on the fluorescence decay kinetics of the donor (Klostermeier and Millar, 2001c). For the hairpin ribozyme, the best fit to the donor decay was obtained using a model of two Gaussian donor-acceptor distance distributions, with mean distances of 34–37 Å and 75–78 Å (N. G. Walter et al., 1999). These distances are in agreement with the corresponding values obtained from the present spFRET experiments (see Results section above). Moreover, the Mg^{2+}-dependent docking efficiencies of 2WJ, 3WJ, and 4WJ ribozyme constructs determined by trFRET are generally in accord with the results shown in Fig. 6. Likewise, the Mg-binding parameters (K_D^{Mg} and n) obtained from the previous trFRET data are also in reasonable agreement with the corresponding values reported here.

Although trFRET and diffusion spFRET provide a consistent view of the overall tertiary folding of the hairpin ribozyme, spFRET is more direct and can provide additional information. For example, the ability to distinguish between one or two ribozyme conformers in the trFRET analysis is based on the goodness of fit obtained using unimodal or bimodal donor-acceptor distance distribution models. In contrast, the evaluation of the spFRET data is model-independent and the number of distinguishable conformers is directly revealed in the FRET efficiency histograms. In addition, the conformer populations are obtained directly

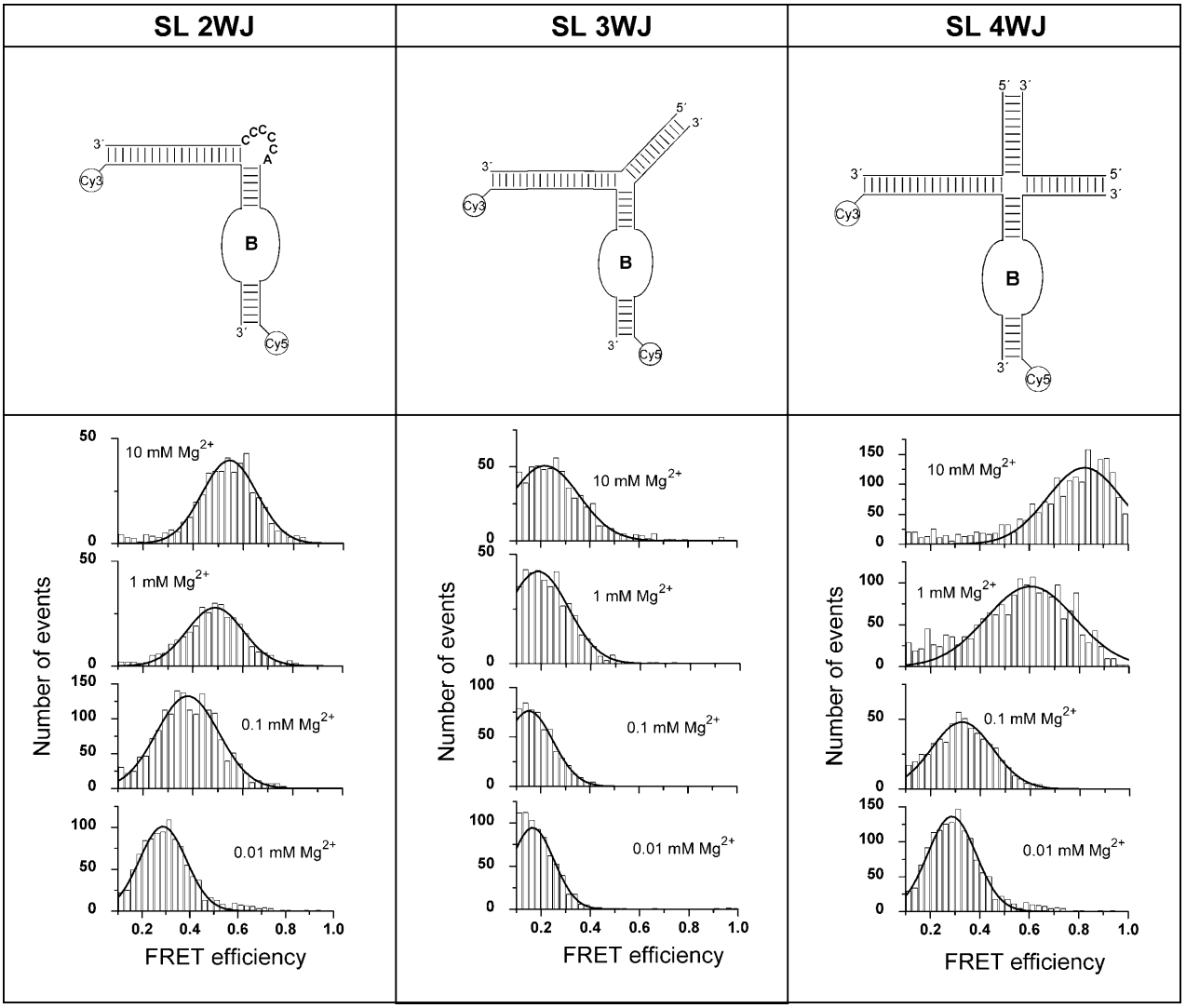

FIGURE 7 Single-loop 2WJ, 3WJ, and 4WJ ribozyme constructs (*upper panel*) and corresponding FRET efficiency histograms at Mg^{2+} concentrations of 0.01, 0.1, 1, and 10 mM (*lower panel*). Data were acquired using a ribozyme concentration of 100 pM in 50 mM Tris/HCl buffer with Mg^{2+} at room temperature, and the data integration time per point was 0.5 ms. The smooth lines show fits using Gaussian functions.

from the areas under each peak in the spFRET histograms, rather than being treated as adjustable parameters in the trFRET analysis. Lastly, kinetic information about equilibrium interconversion of subpopulations (on microsecond to millisecond timescales) is uniquely available from spFRET data.

Evidence for a unique folding intermediate in the 4WJ ribozyme

Our results indicate that the SL 4WJ ribozyme can fold into a compact conformation in the presence of high Mg^{2+} concentrations, with arms A and B juxtaposed in a similar fashion to the docked native 4WJ ribozyme. In striking contrast, neither the 2WJ nor the 3WJ ribozymes can populate such a high-FRET state in the absence of loop A. Since the folding observed in the SL 4WJ ribozyme construct occurs in the absence of loop-loop interactions, the conformational change must be associated with the 4WJ helical junction element itself. Hence, this quasi-docked species must also form in the native 4WJ ribozyme, possibly as a precursor to the specifically docked native state (Fig. 10). Because the two loop-carrying arms are in close proximity, it is likely that the quasi-docked conformation facilitates the formation of tertiary interactions between loops A and B. In fact, by localizing the undocked ensemble close to the native state, the quasi-docked state should reduce the entropic penalty for docking. Consistent with this hypothesis, previous trFRET studies have shown that the 4WJ stabilizes the tertiary structure of the hairpin ribozyme by reducing the entropic penalty for docking as compared with ribozyme constructs containing either a 2WJ or 3WJ

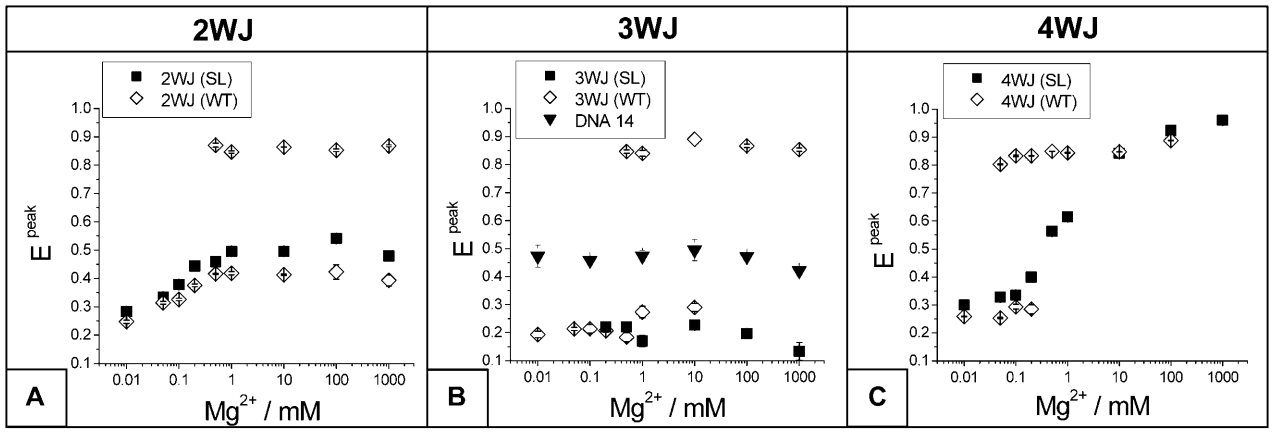

FIGURE 8 Magnesium-induced folding of SL ribozyme constructs. Peak E shifts from the Gaussian fits of the FRET histograms at Mg^{2+} concentrations from 0.01 mM to 1 M for the SL (■) and WT (◇) 2WJ, 3WJ, and 4WJ ribozymes (parts *A*, *B*, and *C*, respectively). Peak E values for a control donor-acceptor labeled DNA molecule with dyes separated by 14 base pairs are shown for comparison as solid triangles in the 3WJ graph in part *B*.

(Klostermeier and Millar, 2000). Additionally, the quasi-docked species appears to form very rapidly (see below), suggesting that this species could act as a kinetic intermediate in the docking pathway of the natural ribozyme. The broad asymmetric peak shape observed for the SL 4WJ implies that extended undocked and quasi-docked states are in rapid conformational exchange, and our kinetic simulations indicate that the rate constant for formation of the quasi-docked state is in the range 10–41 $\times$ 10^3 s^{-1}, whereas the corresponding reverse rate constant is in the range 3.4–14 $\times$ 10^3 s^{-1}. These rates are much faster than the overall rate constant for ribozyme docking observed in previous ensemble kinetic studies, which is on the order of 10^{-2} s^{-1} for a 2WJ ribozyme construct (N. G. Walter et al., 1998). Hence, a quasi-docked conformation could be visited many times during the course of hairpin ribozyme folding, thereby increasing the probability of forming the key tertiary contacts required for stable docking of loops A and B.

A very recent spFRET report on surface-immobilized hairpin ribozymes has also detected a folding intermediate during 4WJ docking (Tan et al., 2003). However, based on the observed FRET efficiency, the two loop-carrying arms appear to be relatively far apart in that species, approximately midway between the extended and docked conformers. In other words, a quasi-docked state was not observed in that work. In contrast, our results imply the presence of a folding intermediate with the two arms in close enough proximity to allow formation of specific loop-loop contacts. Moreover, the quasi-docked species observed in our study appears to form very rapidly, with a rate constant that is two to four orders of magnitude faster than the value reported for formation of the intermediate for the immobilized 4WJ ribozyme under similar conditions (Tan et al., 2003). Currently, we are unable to unambiguously rationalize the difference between the behavior of the immobilized 4WJ ribozyme and the 4WJ construct examined in our solution-based spFRET experiments.

The presence of a quasi-docked conformation potentially complicates the interpretation of FRET data for the hairpin ribozyme. Because of the similar donor-acceptor distances in

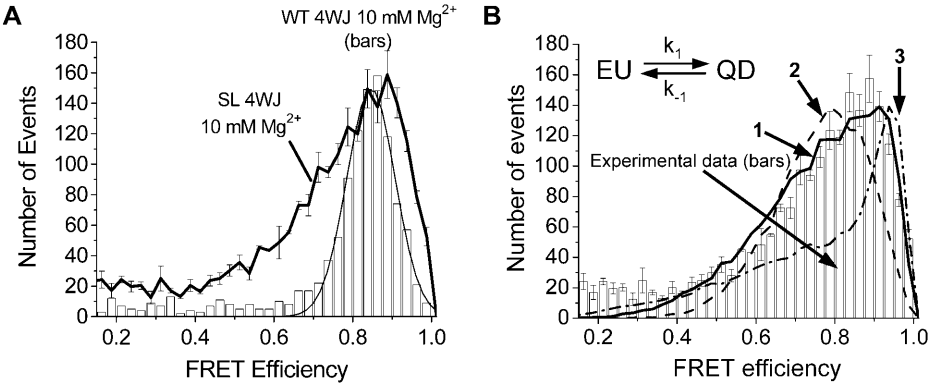

FIGURE 9 Kinetic information from peak shape analysis of spFRET histograms. (*A*) Overlay of FRET efficiency histograms for SL (*bold solid line*) and WT 4WJ (data as *bar graph*, Gaussian fit as *solid line*) ribozymes at 10 mM Mg^{2+}, emphasizing the asymmetric peak shape for the SL 4WJ. The error bars represent single standard deviations. (*B*) Overlay of FRET histograms from two-state simulations (*lines*) and experimental data (*bars*; errors represent single standard deviations) for the SL 4WJ at 10 mM Mg^{2+}. The extended-undocked (*EU*)–quasi-docked (*QD*) equilibrium scheme is shown in the inset. Simulated histograms are shown for forward/reverse (k_1/k_{-1}) rate constants of 20 $\times$ 10^3/6.8 $\times$ 10^3 s^{-1} (*bold solid line, 1*), 41 $\times$ 10^3/14 $\times$ 10^3 s^{-1} (*bold dashed line, 2*), and 10 $\times$ 10^3/3.4 $\times$ 10^3 s^{-1} (*bold dash-dot-dashed line, 3*) with a corresponding equilibrium constant of 3 in favor of the quasi-docked state in all cases. See text for details.

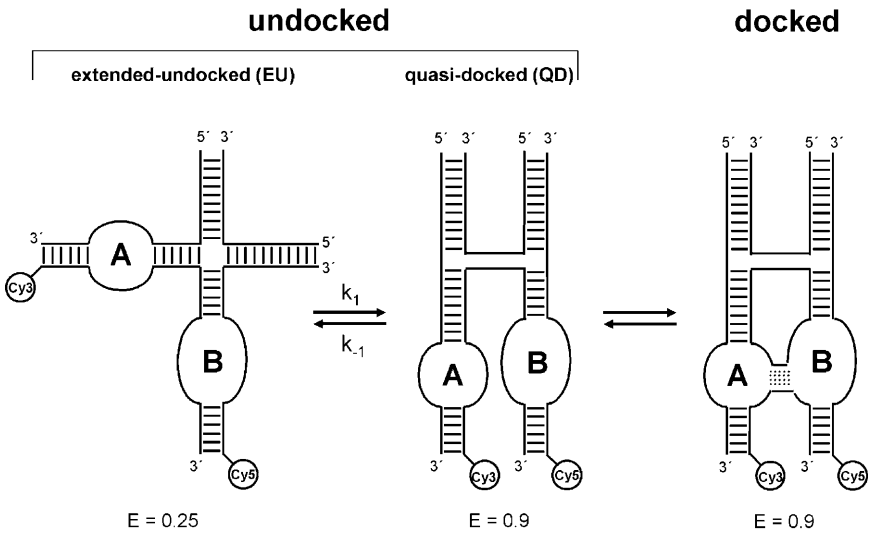

FIGURE 10 Proposed folding pathway for the 4WJ ribozyme. The undocked ensemble shows the equilibrium between the extended-undocked (*EU*) and quasi-docked (*QD*) structures, which is revealed in our spFRET data for the SL 4WJ.

the quasi-docked and specifically-docked conformations, it is difficult to distinguish these two species simply on the basis of the overall FRET efficiency. Similarly, in trFRET experiments, a subpopulation with a short donor-acceptor distance can arise from either specifically-docked or quasi-docked species. One distinguishing feature of the quasi-docked and specifically-docked species, however, is their different kinetic lability. The quasi-docked conformation interconverts rapidly with an extended structure, giving rise to continuous peak shifts with added Mg^{2+}, as well as pronounced asymmetry and broadening in the FRET efficiency histogram at high Mg^{2+} concentrations. In contrast, the specifically-docked conformation (exemplified by the WT 4WJ) is stabilized by an extensive hydrogen bond network (14 hydrogen bonds in all (Rupert and Ferre-D'Amare, 2001)), prolonging the lifetime of this state. As a result, the specifically-docked conformation exchanges only slowly with extended conformations, resulting in a relatively narrow and symmetric peak and an absence of peak shifts in the FRET efficiency histogram. Hence, quasi-docked and specifically-docked ribozyme species are readily distinguished in our diffusion spFRET experiments.

Role of secondary structure elements in tertiary folding

The systematic study of hairpin ribozyme constructs containing different combinations of helical junction and loop elements presented here enables us to define the role of these secondary structural elements during tertiary folding. Clearly, the four-way helical junction in the native ribozyme is the most important determinant for proper folding, guiding the approach of arms A and B. This role is illustrated strikingly by the SL 4WJ, which can fold into a conformation resembling the docked structure even in the absence of loop A. Our results indicate that an early step in the 4WJ ribozyme folding pathway likely involves the formation of a fast equilibrium between extended undocked and quasi-docked structures (Fig. 10). The resultant frequent excursions to this quasidocked structure can facilitate subsequent formation of specific contacts between the two loops, thereby stabilizing the resulting tertiary structure by reducing the entropic penalty for docking. In contrast, the junction geometry plays less of a role in correctly positioning the loops for docking of the less stable 2WJ and 3WJ ribozymes. In fact, the 3WJ ribozyme does not fold significantly (to a compact structure) in the absence of loop A, indicating that the loops are more important than the junction for tertiary folding in this case. Remarkably, the wild-type 3WJ can still form a catalytically active docked conformation, presumably by trapping a small population of molecules that transiently occupy a compact structure. For the 2WJ, some folding is observed in the absence of loop A, although the molecule does not form a stable quasi-docked conformation with arms A and B in close proximity. Hence, both the junction and the loops are important for tertiary folding of the 2WJ ribozyme. The inability of two- and three-way helical junctions to populate stable quasi-docked conformations appears to be a key determinant for the reduced stability and incomplete tertiary folding observed in the corresponding ribozymes. In summary, our comparative study of different ribozyme constructs shows that in contrast with the 2WJ and the 3WJ, the natural 4WJ architecture can efficiently guide conformational search events during ribozyme folding, thereby dramatically influencing subsequent tertiary structure formation and stability. Our results also highlight the ability of the diffusion spFRET method to resolve conformational subpopulations important during the course of RNA folding.

We thank Dagmar Klostermeier for assistance in preparing some of the hairpin ribozyme constructs.

This work was supported by grants from the National Institutes of Health to D.P.M. (grant no. GM58873) and A.A.D. (grant no. GM066833).

REFERENCES

Buchmueller, K. L., A. E. Webb, D. A. Richardson, and K. M. Weeks. 2000. A collapsed non-native RNA folding state. *Nat. Struct. Biol.* 7:362–366.

Dahan, M., A. A. Deniz, T. J. Ha, D. S. Chemla, P. G. Schultz, and S. Weiss. 1999. Ratiometric measurement and identification of single diffusing molecules. *Chem. Phys.* 247:85–106.

Deniz, A. A., M. Dahan, J. R. Grunwell, T. Ha, A. E. Faulhaber, D. S. Chemla, S. Weiss, and P. G. Schultz. 1999. Single-pair fluorescence resonance energy transfer on freely diffusing molecules: observation of Forster distance dependence and subpopulations. *Proc. Natl. Acad. Sci. USA.* 96:3670–3675.

Deniz, A. A., T. A. Laurence, G. S. Beligere, M. Dahan, A. B. Martin, D. S. Chemla, P. E. Dawson, P. G. Schultz, and S. Weiss. 2000. Single-molecule protein folding: diffusion fluorescence resonance energy transfer studies of the denaturation of chymotrypsin inhibitor 2. *Proc. Natl. Acad. Sci. USA.* 97:5179–5184.

Deniz, A. A., T. A. Laurence, M. Dahan, D. S. Chemla, P. G. Schultz, and S. Weiss. 2001. Ratiometric single-molecule studies of freely diffusing biomolecules. *Annu. Rev. Phys. Chem.* 52:233–253.

Fang, X. W., T. Pan, and T. R. Sosnick. 1999. Mg^{2+}-dependent folding of a large ribozyme without kinetic traps. *Nat. Struct. Biol.* 6:1091–1095.

Fang, X. W., P. Thiyagarajan, T. R. Sosnick, and T. Pan. 2002. The rate-limiting step in the folding of a large ribozyme without kinetic traps. *Proc. Natl. Acad. Sci. USA.* 99:8518–8523.

Grunwell, J. R., J. L. Glass, T. D. Lacoste, A. A. Deniz, D. S. Chemla, and P. G. Schultz. 2001. Monitoring the conformational fluctuations of DNA hairpins using single-pair fluorescence resonance energy transfer. *J. Am. Chem. Soc.* 123:4295–4303.

Ha, T. 2001. Single-molecule fluorescence methods for the study of nucleic acids. *Curr. Opin. Struct. Biol.* 11:287–292.

Ha, T., T. Enderle, D. F. Ogletree, D. S. Chemla, P. R. Selvin, and S. Weiss. 1996. Probing the interaction between two single molecules: fluorescence resonance energy transfer between a single donor and a single acceptor. *Proc. Natl. Acad. Sci. USA.* 93:6264–6268.

Ha, T., X. Zhuang, H. D. Kim, J. W. Orr, J. R. Williamson, and S. Chu. 1999. Ligand-induced conformational changes observed in single RNA molecules. *Proc. Natl. Acad. Sci. USA.* 96:9077–9082.

Klostermeier, D., and D. P. Millar. 2000. Helical junctions as determinants for RNA folding: origin of tertiary structure stability of the hairpin ribozyme. *Biochemistry.* 39:12970–12978.

Klostermeier, D., and D. P. Millar. 2001a. Tertiary structure stability of the hairpin ribozyme in its natural and minimal forms: different energetic contributions from a ribose zipper motif. *Biochemistry.* 40:11211–11218.

Klostermeier, D., and D. P. Millar. 2001b. RNA conformation and folding studied with fluorescence resonance energy transfer. *Methods.* 23:240–254.

Klostermeier, D., and D. P. Millar. 2001c. Time-resolved fluorescence resonance energy transfer: a versatile tool for the analysis of nucleic acids. *Biopolymers.* 61:159–179.

Klostermeier, D., and D. P. Millar. 2002. Energetics of hydrogen bond networks in RNA: Hydrogen bonds surrounding G+1 and U42 are the major determinants for the tertiary structure stability of the hairpin ribozyme. *Biochemistry.* 41:14095–14102.

Murchie, A. I., J. B. Thomson, F. Walter, and D. M. Lilley. 1998. Folding of the hairpin ribozyme in its natural conformation achieves close physical proximity of the loops. *Mol. Cell.* 1:873–881.

Rupert, P. B., and A. R. Ferre-D'Amare. 2001. Crystal structure of a hairpin ribozyme-inhibitor complex with implications for catalysis. *Nature.* 410:780–786.

Russell, R., I. S. Millett, S. Doniach, and D. Herschlag. 2000. Small angle X-ray scattering reveals a compact intermediate in RNA folding. *Nat. Struct. Biol.* 7:367–370.

Russell, R., X. Zhuang, H. P. Babcock, I. S. Millett, S. Doniach, S. Chu, and D. Herschlag. 2002a. Exploring the folding landscape of a structured RNA. *Proc. Natl. Acad. Sci. USA.* 99:155–160.

Russell, R., I. S. Millett, M. W. Tate, L. W. Kwok, B. Nakatani, S. M. Gruner, S. G. Mochrie, V. Pande, S. Doniach, D. Herschlag, and L. Pollack. 2002b. Rapid compaction during RNA folding. *Proc. Natl. Acad. Sci. USA.* 99:4266–4271.

Selvin, P. R. 2000. The renaissance of fluorescence resonance energy transfer. *Nat. Struct. Biol.* 7:730–734.

Sosnick, T. R., and T. Pan. 2003. RNA folding: models and perspectives. *Curr. Opin. Struct. Biol.* 13:309–316.

Stryer, L., and R. P. Haugland. 1967. Energy transfer: a spectroscopic ruler. *Proc. Natl. Acad. Sci. USA.* 58:719–726.

Tan, E., T. J. Wilson, M. K. Nahas, R. M. Clegg, D. M. J. Lilley, and T. Ha. 2003. A four-way junction accelerates hairpin ribozyme folding via a discrete intermediate. *Proc. Natl. Acad. Sci. USA.* 100:9308–9313.

Treiber, D. K., and J. R. Williamson. 1999. Exposing the kinetic traps in RNA folding. *Curr. Opin. Struct. Biol.* 9:339–345.

Treiber, D. K., and J. R. Williamson. 2001. Beyond kinetic traps in RNA folding. *Curr. Opin. Struct. Biol.* 11:309–314.

Walter, F., A. I. Murchie, and D. M. Lilley. 1998. Folding of the four-way RNA junction of the hairpin ribozyme. *Biochemistry.* 37:17629–17636.

Walter, N. G., J. M. Burke, and D. P. Millar. 1999. Stability of hairpin ribozyme tertiary structure is governed by the interdomain junction. *Nat. Struct. Biol.* 6:544–549.

Walter, N. G., K. J. Hampel, K. M. Brown, and J. M. Burke. 1998. Tertiary structure formation in the hairpin ribozyme monitored by fluorescence resonance energy transfer. *EMBO J.* 17:2378–2391.

Weiss, S. 2000. Measuring conformational dynamics of biomolecules by single molecule fluorescence spectroscopy. *Nat. Struct. Biol.* 7:724–729.

Zhuang, X., L. E. Bartley, H. P. Babcock, R. Russell, T. Ha, D. Herschlag, and S. Chu. 2000. A single-molecule study of RNA catalysis and folding. *Science.* 288:2048–2051.

Zhuang, X., H. Kim, M. J. Pereira, H. P. Babcock, N. G. Walter, and S. Chu. 2002. Correlating structural dynamics and function in single ribozyme molecules. *Science.* 296:1473–1476.